European sulphate aerosols were a key driver of the early twentieth-century intensification of the Asian summer monsoon

Weihao Sun[1,2], Massimo A. Bollasina[3], Ioana Colfescu[4,5], Guoxiong Wu[6] and Yimin Liu[6]

[1]East China Sea Forecasting and Disaster Reduction Center, Ministry of Natural Resources, Shanghai, China
[2]Observation and Research Station of Huaniaoshan East China Sea Ocean-Atmosphere Integrated Ecosystem, Ministry of Natural Resources, Shanghai, China
[3]School of GeoSciences, University of Edinburgh, Edinburgh, UK
[4]School of Mathematics and Statistics, University of St Andrews, St Andrews, UK
[5]National Centre for Atmospheric Science, UK
[6]Key Laboratory of Earth System Numerical Modelling and Application, Institute of Atmospheric Physics, Chinese Academy of Sciences, Beijing, China

~~Weihao Sun[1,2], Massimo A. Bollasina[1], Ioana Colfescu[3,4], Guoxiong Wu[2] and Yimin Liu[2]~~

~~[1]School of GeoSciences, University of Edinburgh, Edinburgh, UK~~
~~[2]Key Laboratory of Earth System Numerical Modelling and Application, Institute of Atmospheric Physics, Chinese Academy of Sciences, Beijing, China.~~
~~[3]School of Mathematics and Statistics, University of St Andrews, St Andrews, UK~~
~~[4]National Centre for Atmospheric Science, UK~~

Correspondence to: Massimo A. Bollasina (Massimo.Bollasina@ed.ac.uk)

Abstract. Observations show that the Asian summer monsoon experienced substantial multi-decadal changes during the early 20th century, including a wetting trend over South Asia and a southward rainfall shift over East Asia. Despite their significance, these variations have received limited attention, and the underlying mechanisms remain poorly understood. This study investigates the role of increased European sulphate aerosol emissions in shaping these monsoon changes using ensemble experiments with the Community Earth System Model. The aerosol-driven rainfall patterns over South and East Asia resemble observations, suggesting that European aerosols played an important role in modulating the monsoon. These changes are linked to large-scale anomalies in surface climate and three-dimensional atmospheric circulation across the Indo-Pacific, which alter moisture transport to the continent, the main driver of the rainfall anomalies. Regional circulation anomalies form part of a hemispheric upper-tropospheric wave train originating over central Europe and extending through the Middle East to the Pacific. The wave train arises as a thermodynamic adjustment to the aerosol-induced surface cooling and

related anticyclone over Europe, extends to the upper troposphere, and, while propagating eastward, induces three-dimensional circulation anomalies across Asia that affect the monsoon. These findings provide compelling evidence for the influence of European sulphate aerosols on the early 20th-century monsoon variability, which is relevant for improving current understanding of the regional-scale impacts of anthropogenic aerosols. As European SO_2 emissions continue to decline, this study sheds light upon a possible ongoing and future pathway which may significantly modulate the monsoon response to Asian aerosol changes.

1 Introduction

The Asian summer monsoon (ASM) is a vital source of water for over 60% of the world's population (Turner and Annamalai, 2012). Its interannual variability and long-term changes have significant implications for water resources, agriculture, and economic activities across Asia (e.g., Gadgil and Rupa Kumar, 2006).

In the past decade, anthropogenic aerosols have attracted considerable scientific interest due to their ability to offset part of the warming caused by greenhouse gases (GHGs) (e.g., Samset et al., 2018; Hegerl et al., 2019; Li et al., 2022). Aerosols influence climate by scattering and absorbing solar radiation, and by acting as cloud condensation and ice nuclei, thereby modifying cloud albedo, lifetime, and precipitation processes (Boucher et al., 2013; Stier et al., 2024). They remain the largest source of uncertainty in estimating anthropogenic climate forcing since the pre-industrial era (Andrews and Forster, 2020; Bellouin et al., 2020). While their global historical effective radiative forcing is smaller than that of GHGs, aerosols can trigger strong regional climate responses due to their spatial and temporal variability (e.g., Szopa et al., 2021).

The link between long-term changes in aerosol emissions and ASM variability is widely debated (e.g., Lau 2016; Li et al., 2016; Wu et al., 2016). Research is particularly challenging due to the compounding effects of internal variability, model biases, and divergent model responses (e.g., Saha and Gosh, 2019; Liu et al., 2024). Nonetheless, studies using observational and modelling evidence have highlighted the significant impact of aerosols, both regional (i.e., Asian-only) and remote (i.e., outside Asia), on the late 20th century weakening of the South ASM and the emergence of a southern-flood-northern-drought (SFND) pattern over East Asia (e.g., Bollasina et al., 2011; Guo et al., 2013; Salzmann et al., 2014; Li et al., 2015; Dong et al. 2019; Wilcox et al. 2020).

Gauge records reveal clear multi-decadal variability in both South Asian and East Asian summer monsoons throughout the 20th century (e.g., Zhang and Zhou, 2011; Preethi et al., 2017; Li et al., 2023). In particular, the first half of the century saw an increase in rainfall over South Asia, most notably in central India, and a tripole pattern over East Asia, with excess rainfall in the south and northeast, and drier conditions along the Yangtze River basin. These anomalies appear to be part of a coherent ASM-wide fluctuation, mirrored in broader Norhern Hemispheric summer monsoon changes (Zhang and Zhou, 2011; Preethi et al., 2017; Wang et al., 2018; Goswami et al., 2023). Strikingly, this pattern reversed in the second half of the 20th century, producing comparable but opposite sign anomalies, and resulting in minimal net change over the full period.

While monsoon changes since the 1950s have been extensively studied (e.g., Bollasina et al., 2011; Salzmann et al., 2014; Song et al., 2014; Liu et al., 2019; Liu et al., 2024; Shao et al., 2024), early-century variations have received less attention. Yet, given the contrasting trends throughout the historical period, understanding monsoon drivers and the underpinning physical mechanisms in the entire record is essential to constrain the nature of its multi-decadal variability and improve future projections. This is particularly relevant in the context of disentangling internal climate variability from externally-forced changes (e.g., Salzmann and Cherian, 2015; Huang et al., 2020). In this regard, compared to the later period, it is conceivable to assume a negligible role of Asian aerosols in the first half of the 20th century, as emissions underwent a significant growth only from the 1950s and a sharp rise after the 1970s (Smith et al., 2011; Lund et al., 2019). In contrast, North American and European aerosols had already increased substantially, raising the possibility of their significant influence on the monsoon.

Several studies have highlighted the potential role of remote, including European, aerosols in driving Asian summer monsoon changes (e.g., Cowan and Cai, 2011; Bollasina et al., 2014; Guo et al., 2015; Dong et al., 2016; Liu et al., 2018; Shawki et al., 2018; Undorf et al., 2018a,b; Westervelt et al., 2018; Wang et al., 2020). However, these analyses often relied on idealised simulations, such as long equilibrium experiments with present-day emissions turned on or off. Whether aerosol influences were already detectable in the early 20th century remains an open question. Addressing this gap is crucial for better understanding and narrowing uncertainty in aerosol-related future monsoon projections, especially considering divergent present-day emission trends (e.g., Wang et

al., 2021a) and a wide range of plausible future pathways (Samset et al., 2019; Persad et al., 2023).

Against this backdrop, this study investigates whether rising European sulphate aerosols – the dominant anthropogenic aerosol species of the region (e.g., Hoesly et al., 2018) – had any detectable impact on the ASM during the first half of the 20th century. Section 2 introduces the climate model, experimental setup, and observational data used. Section 3 presents the ASM response and examines the underlying mechanism. Discussion and conclusions are provided in Section 4.

2 Data and methods

The primary data comprises output from two transient historical (1850–2005) experiments with the fully coupled Community Earth System Model (CESM) version 1.2.2 (Hurrell et al., 2013). The atmospheric component is the Community Atmospheric Model version 5.3 (CAM5.3, Neale et al., 2012), which includes a 3-mode aerosol scheme and a prognostic representation of aerosol-cloud interactions (Ghan et al., 2012). The horizontal resolutions are 1.9° x 2.5° for the atmosphere and 0.6° x 0.9° for the ocean. The model reproduces spatial patterns and magnitude of the climatological summertime monsoon rainfall and low-tropospheric circulation reasonably well (Supplementary ~~Fig.~~ Figure S1), consistent with the overall performance of CMIP5/CMIP6 models (Meehl et al., 2020; He et al., 2023). A full description of the model and experiments is provided by Undorf et al. (2018a); here, we briefly summarise key details.

Each experiment consists of an 8-member ensemble initialised from different points in a 200-year pre-industrial (PI) simulation with fixed anthropogenic emissions at 1850 levels. The first experiment (ALL) includes time-varying historical emissions of anthropogenic aerosols, greenhouse gases, and natural forcing factors. The second (fixEU) is identical to ALL except that anthropogenic SO_2 and SO_4 emissions over Europe (EU) are held at PI levels. Europe is defined according to Tier 1 regions from the Hemispheric Transport of Air Pollution 2 experiments (Koffi et al., 2016).

Several observational datasets are also used. Precipitation was taken from three land-only monthly gridded gauge-based datasets to account for uncertainties and discrepancies: the 1° x 1° Global Precipitation Climatology Centre

v2020 (GPCC; Schneider et al., 2014), the 0.5° x 0.5° Climate Research Unit v4.00 (CRU; Harris et al., 2014), and the 0.5° x 0.5° University of Delaware v401 (UDEL, Willmott and Matsuura, 1995). Monthly sea level pressure surface is from the 5° x 5° Hadley Centre Sea Level Pressure dataset (HadSLP2; Allan and Ansell, 2006), and 850-hPa winds from the ECMWF Reanalysis 5 (Hersbach et al., 2020). Monthly observed precipitation from the 2.5° x 2.5° Climate Prediction Center Merged Analysis of Precipitation dataset (CMAP, Xie and Arkin, 2017) is also used for model validation.

The analysis focuses on the summer (June–August, JJA) monsoon variation during the early 20th century. Temporal changes are estimated using least-squares linear trends from 1901 to 1955. Alternative trend estimation methods (i.e., Sen's non-parametric slope or differences between the 1941–1955 and 1901–1915 means) yield similar results (not shown). As the main objective is to isolate the influence of external forcing, particularly anthropogenic aerosols, on the ASM, changes are primarily assessed using ensemble means. Assuming linear additivity of responses, the difference between the ALL and fixEU experiments is interpreted as the impact of European SO_2 emissions. Statistical significance is assessed using a two-tailed Student's *t*-test at the 90% confidence level. To identify the contribution of the model's internal variability to the forced response, individual ensemble members are also examined. Additionally, the PI simulation is used to assess the statistical significance of the forced changes relative to internal variability. We generate 10,000 bootstrap samples of 8-member ensemble means to construct the probability distribution of unforced linear trends; the 90% confidence interval is defined as the range within which 90% of these fall.

3 Results

3.1 Observed and simulated precipitation trends

Observational data show that JJA precipitation changes across Asia during the first half of the twentieth century exhibit a coherent large-scale pattern (~~Fig.~~ Figure 1a), with robust features across multiple datasets (Supplementary ~~Fig.~~ Figure S2). Over South Asia, significant wetting is observed across central and northern India, contrasted by drying over southern and northeastern India, the eastern Himalayas and northern Myanmar. Further east, rainfall deficits occur over southern Indochina and Indonesia, with a pronounced drying over the middle and lower reaches of the Yangtze River valley (105°–120°E, 25°–35°N). In contrast, precipitation increases are seen in a band extending from northern Indochina through southern China, and further north into northwestern

China and the Korean peninsula. Interestingly, the anomalous rainfall pattern over South Asia closely resembles, but with opposite sign, that associated with the late 20th century weakening of the monsoon, while the anomalies over eastern Asia are reminiscent of the reversed SFND pattern (e.g., Bollasina et al., 2011; Dong et al., 2016).

To provide further context on the long-term precipitation variations, Figure 1c shows the observed time series of monsoon rainfall anomalies over the core Indian monsoon region (75°–87°E, 16°–27°N land-only points, see box in ~~Fig.~~ Figure 1c). Beyond interannual and decadal fluctuations, the record reveals a marked increase from the 1900s to the mid–1950s (+0.55/+0.76 mm day^{-1} in GPCC/CRU over 55 years, statistically significant at the 90% confidence level), equivalent to about 7–11% of the long-term climatology. The anomaly also results in a 5–7% increase in the All–India rainfall relative to early–century values. A similar analysis over southern China (110°–120°E, 25°–35°N; Supplementary ~~Fig.~~ Figure S3) also shows a prominent, statistically significant, multi-decadal trend.

Despite its coarser resolution, the ALL ensemble mean captures the main spatio-temporal characteristics of the observed precipitation trends, although amounts are generally smaller (~~Fig.~~ Figure 1b). The model reproduces the observed widespread precipitation increase over northern India, albeit with a weaker magnitude (+0.14 mm day^{-1} (55 years)$^{-1}$ over the core region) and a slight eastward shift, and the drying over southern India. The model likely underrepresents the full extent of the interaction with the Western Ghats. The simulated rainfall dipole over eastern China aligns with observations, although the amounts are slightly underestimated. However, the model fails to reproduce the observed wetting over southern China and northern Indochina, possibly due to limitations in resolving interactions with the complex terrain. The sign of the core precipitation anomalies over India is consistent across most of the individual ensemble members (6 out of 8), supporting a dominant anthropogenic origin (Supplementary ~~Fig.~~ Figure S4).

Preventing European sulphate aerosols from increasing results in drier conditions over central-northern India and the northern Bay of Bengal (BoB), with wetting over the eastern Himalayas and Myanmar. Concurrently, the precipitation anomalies over eastern Asia reverse polarity, while a pronounced precipitation deficit appears over Indochina. As a result, the precipitation pattern associated with increased European SO_2 emissions closely resembles observations and shows greater similarity than ALL across Asia. The aerosol-related precipitation

response is also robust across most of the ensemble members (Supplementary ~~Fig.~~ Figure S4). For example, the ensemble-mean rainfall trend over the core Indian region amounts to +0.33 mm day^{-1} over 55 years, with increases in 6 out of 8 ensemble members. This indicates that European aerosols substantially contributed to the early 20th-century ASM rainfall trends.

The observed and simulated 55-year rainfall trends over central-northern India are also compared with the corresponding range of trends from the PI experiment (Supplementary Figure~~s.~~ S4~~) and S5~~). The trend from CRU is outside the respective 90% confidence interval, while it is slightly below in GPCC. The trend from the ALL-ensemble mean is within the corresponding 90% confidence interval (+0.19 mm day^{-1} over 55 years; Supplementary Figure S5), although five of its members exhibit positive trends that are markedly discernible from internal variability. The ensemble-mean drying trend in the fixEU experiment exceeds the 90% confidence level. As a result, the ensemble-mean trend associated with European aerosols (EU) is clearly distinguishable from internally-generated fluctuations, even exceeding the 95% confidence level (+0.24 mm day^{-1} over 55 years).

3.2 Changes in the monsoon circulation

Changes in precipitation across Asia are closely linked with variations in near-surface and atmospheric circulation patterns (~~Fig.~~ Figure 2). The spatial correspondence between wet (dry) anomalies and regions of moisture flux convergence (divergence) underscores the dominant role of circulation-induced moisture transport in shaping monsoon precipitation trends (~~Fig.~~ Figure 2b). Over South Asia, a prominent anomalous anticyclone centred over southern India and the western BoB characterises the low-tropospheric flow. Over East Asia and the western Pacific, a zonal dipole emerges: an anomalous cyclone spans northern Indochina, southeastern China, and the South China Sea, accompanied by an elongated anticyclone extending from central China to the western Pacific.

As Figure 2a shows, strong low-level easterlies across southern India oppose the climatological westerlies from the Arabian Sea, leading to local rainfall deficits. Meanwhile, the climatological moisture-laden southwesterlies are deflected northward over the northern Arabian Sea. Upon reaching central and northern India, this flow converges with anomalous northeasterlies from northern Indochina and the northern BoB, enhancing rainfall (~~Fig.~~ Figure 2b). On the western flank of the anomalous Indo-Pakistan low, dry northerlies suppress precipitation over Pakistan. Over East Asia, enhanced Pacific moisture transport into southern China and northeastern Indochina, opposing the climatological southerlies linked to the western Pacific subtropical high, leads to regional wetting.

Return westerlies south of the anomalous Pacific low further reinforce the moisture flux from the BoB, contributing to widespread wetting across the Bay and northwestern Indochina. In contrast, reduced southerly moisture advection brings drying to southern Indonesia and northeastern China.

Figure 2c shows that the regional upper-tropospheric circulation also exhibits substantial changes, consistent with the tropical balance among convective heating, ascent, and upper-level divergence (and vice versa). Over northern India and the northern BoB, strong mid-tropospheric ascent coincides with rainfall enhancement, accompanied by divergent outflow in the upper troposphere. One branch heads northeastward, converging and subsiding over Burma and central China. Other branches are directed southwestward and southward, with corresponding mid-tropospheric subsidence and surface anticyclones over southern India and the northern equatorial Maritime Continent. A meridional system of divergent cells over East Asia and the western Pacific reflects the deep convection and upper-tropospheric divergence centred near 20°N. The southern cell also converges and subsides over the north equatorial Maritime Continent, aligning with the southern outflow from South Asia.

3.3 Aerosol forcing over Europe

To elucidate the generating mechanism, Figure 3a shows the widespread sulphate loading anomaly over Europe resulting from enhanced emissions. Once emitted, aerosols are transported across and beyond the Continent. Notably, aerosols spread southwestward towards northern Africa and the tropical Atlantic via the summertime climatological circulation of the Azores high, and eastward over central Eurasia by the midlatitude climatological westerlies, displacing the maximum loading and Aerosol Optical Depth (AOD; ~~(~~Supplementary Figure S6~~not shown~~) eastward of the emissions source.

Consistent with this transport, surface clear-sky downward shortwave radiation decreases across Europe, with anomalies exceeding -3 W m^{-2} over 55 years in regions of peak aerosol loading (~~Fig.~~ Figure 3b), accounting for approximately 80% of the local reduction in the all-sky radiation (Supplementary ~~Fig.~~ Figure S6). All-sky radiation anomalies are larger (up to -5 W m^{-2}) due to increased cloudiness associated with circulation changes (see last paragraph in this Section~~ter~~). As expected by the aerosol scattering effect, net shortwave differences between the top-of-atmosphere and surface are minimal (Supplementary Figure S6~~not shown~~). Including longwave effects, the net radiative cooling at the model top reached about -2 W m^{-2} over central and eastern Europe (Supplementary Figure~~.~~ S6).

Cloud droplet number concentration displays widespread positive anomalies over central and eastern Europe concurrently with a negative, albeit weak, decrease in cloud top effective radius (Supplementary ~~Fig.~~ Figure S6). These changes are consistent with those expected by the cloud response to sulphate aerosols, assuming negligible variations in water liquid content. The latter remains relatively unchanged or slightly enhanced due to anomalous northwesterlies from the Atlantic (see next paragraph~~below~~).

As a result of the aerosol-induced dimming, near-surface temperature shows anomalous cooling over central and eastern Europe (~~Fig.~~ Figure 3c), and concurrently, the circulation adjusts thermodynamically, with marked anticyclonic anomalies occurring at the surface. Interestingly, ~~Fig.~~ Figure 3d shows that the largest cooling and the high-pressure core are displaced east of the aerosol loading maximum, suggesting the combined influence of direct forcing, feedbacks, and modulation by the climatological flow. For example, eastward aerosol transport and temperature advection by the climatological westerlies contribute in concert to displacing the aerosol cooling to the east. The associated northeasterly flow on the eastern flank of the surface anticyclone further reinforces the cooling over eastern Europe. Note that the simulated northeastward displacement of the anomalous anticyclone is consistent with the displacement shown by ~~pattern of~~ observed sea-level pressure trends (Supplementary ~~Fig.~~ Figure S7).

3.4 Rossby wave propagation and remote teleconnections

As shown in Figure 4, the regional signature of European aerosols extends to the mid and upper troposphere. Streamfunction anomalies feature a (weak) equivalent-barotropic nature and a slight northwestward tilt with height (not shown), consistent with the mature phase of an extratropical disturbance. At 300 hPa, anticyclonic anomalies are seen over central Europe. This pattern forms part of a wave train signal extending across the northern hemisphere, indicating a Rossby wave response to increased European aerosols and related upper-level relative vorticity anomalies, which serve as the primary source of wave activity.

Upper-level meridional wind anomalies align with expectations from the streamfunction/geopotential height pattern, revealing alternating cyclonic and anticyclonic centres (~~Fig.~~ Figure 4b). The wave activity flux (e.g., Takaya and Nakamura 2001) highlights two eastward propagation branches. The main branch extends southeastward across the Middle East to Pakistan and northwestern India, where it weakens while turning

northeastward into eastern China and converges over Japan. This flux follows the Asian jet stream, which acts as a Rossby waveguide. A secondary, weaker high-latitude pathway is also evident: the wave flux points northeastward towards northern Russia, crosses northern Eurasia, and then turns southeastward over the northwestern Pacific, ultimately converging with the main pathway.

Mid-tropospheric ascent and descent anomalies accompany the wave train (~~Fig.~~ Figure 4b), consistent with the vorticity balance (e.g., Rodwell and Hoskins 2001). For example, the anticyclonic anomaly over Afghanistan and Pakistan induces southward flow and subsidence to its east, suppressing precipitation over Pakistan and the western Tibetan Plateau. Conversely, an anomalous upper-tropospheric anticyclone develops over eastern China and the western Pacific (120°-140°E). Northward flow and ascent occur on its western flank, while subsidence is found to the east, in agreement with the fundamental vorticity balance. At lower levels, this configuration generates an anomalous westerly flow from the western Pacific toward south-eastern China, enhancing moisture transport and producing a positive precipitation anomaly. This rainfall anomaly, in turn, drives strong variations in the tropical divergent circulation: part of the divergent outflow extends toward the Maritime Continent, where it converges, descends, and produces anomalous anticyclonic flow. The interaction between extratropical wave-induced anomalies over eastern China/western Pacific and the resulting meridional adjustments in the tropical divergent circulation account for the characteristic tripolar anomalous rainfall pattern across East Asia. ~~over southern China, near-surface low-pressure anomalies, upward motion, and increased precipitation are associated with northward flow.~~ These results suggest that key upper-tropospheric action centres, over the Middle East and southern China/western Pacific, initiate low-tropospheric circulation adjustments that generate the anomalous rainfall pattern across Asia.

4 Discussion and concluding remarks

The Asian summer monsoon hydroclimate underwent significant changes in the early 20th century, characterised by a wetting trend over South Asia and a southern rainfall shift over East Asia. This study finds that increased European anthropogenic sulphate aerosols played a key role in driving these observed monsoon changes. The aerosol-induced cooling and large-scale anticyclonic anomaly over central/eastern Europe extend from the surface to the upper troposphere. These anomalies trigger subsequent atmospheric circulation adjustments in the form of an eastward propagating Rossby-wave train, which is central to realising the remote aerosol impact across Asia.

These findings shed new light on the drivers and mechanisms of monsoon multidecadal variability. While most existing research has focused on recent monsoon changes, the early historical period remains unexplored. Moreover, many prior studies have relied on long, equilibrium-type experiments to enhance the signal-to-noise ratio, but these are less representative of the transient response to evolving aerosol emissions. An atmospheric propagation pathway similar to the one identified here has been discussed in earlier literature, particularly in relation to the downstream signature of the North Atlantic Oscillation (e.g., Watanabe 2004) and broader teleconnections between Europe and East Asia (e.g., Lu et al. 2002; Enomoto et al., 2003), yet it has been largely overlooked in the context of aerosol forcing (e.g., Wang et al., 2021b), which has instead typically emphasised changes in the large-scale meridional temperature gradient across Eurasia as the dominant key mechanism.

Placing our study within the broader literature on remote aerosol-monsoon interactions underscores its relevance. Cowan and Cai (2011) were among the first to identify the influence of non-Asian aerosols, primarily European sulphate, in weakening the ASM over the 20th century by inducing widespread Eurasian cooling and thereby reducing the meridional temperature gradient, which in turn weakens the southerly monsoon flow. Similarly, Guo et al. (2015, 2016) linked widespread drying across Asia to increased global aerosol emissions, mainly from non-Asian sources, and the subsequent modulation of the zonal-mean meridional temperature gradient. Focusing on the fast, atmospheric-only equilibrium response to the removal of European aerosols, Dong et al. (2016) reported a strengthening of the South Asian monsoon and a southern shift in East Asian rainfall, attributed to the downstream advection of cooler, drier air from Europe to Asia and consequent weakening of the tropospheric thermal gradient. Shawki et al. (2018) similarly found that removing European aerosol emissions strengthens, albeit weakly, the South Asian monsoon and shifts the East Asian monsoon northward, via changes in the large-scale temperature gradient and the interhemispheric heat and moisture transport. Liu et al. (2018) reported a slight decrease in annual mean precipitation over Asia associated with increased European sulphate aerosols, driven by the slow (ocean-mediated) component of the total response via inter-hemispheric heating redistribution. Similar rainfall patterns were also shown by Westervelt et al. (2018). More recently, Wang et al. (2017) and Wang et al. (2020) highlighted that non-local aerosol emissions are as influential as local ones in weakening the East Asian summer monsoon, primarily through easterly advection of colder air across Eurasia and resulting change in meridional heat transport, in agreement with Dong et al. (2016).

An enhanced meridional temperature gradient between central Eurasia and the IO is a well-known contributor to stronger monsoon precipitation over South Asia (e.g., Meehl and Arblaster, 2002). Indeed, this has been identified, for example, as one of the elements contributing to enhanced future monsoon precipitation by the end of the 21st century (e.g., Meehl et al., 2024). This outcome, however, is not borne out in our study, as the mid and high troposphere temperature averaged over the 60°-100°E sector displays enhanced cooling compared to the north-equatorial IO, resulting in a weaker meridional temperature gradient (not shown). This discrepancy indicates that the aerosol-induced regional monsoon circulation and precipitation variations over South Asia cannot be explained by broad-scale sector-mean temperature changes. On the contrary, the anomalous temperature pattern over Eurasia displays a close relationship with that induced by the anomalies in atmospheric advection, especially in the meridional direction, in turn associated with the upper-tropospheric wave train.

This dynamical pathway and the critical role of large-scale remotely driven atmospheric dynamical changes finds support in Bollasina et al. (2014). Although secondary to regional emissions in explaining the recent monsoon rainfall decline, extratropical aerosols were nonetheless shown to induce widespread temperature and wind anomalies across Asia, revealing the complex interplay between aerosol forcing, precipitation, and circulation changes. Undorf et al. (2018a, b) also highlighted the importance of midlatitude aerosol forcing in explaining the observed weakening of the South Asian monsoon through the mid-1970s, underscoring the key role of Eurasian-scale dynamical adjustments.

An important question is whether Indian Ocean (IO) SSTs also influenced the monsoon. The ALL ensemble, consistent with the overall performance of CMIP5/6 models (e.g., Roxy et al., 2014), exhibits widespread and relatively homogeneous warming across the basin. In contrast, aerosol-induced SST trends, albeit weak, show warming over the western equatorial IO and cooling over the subequatorial regions (Supplementary Fig~~.~~ure S8). This cross-equatorial dipole in SST trends is also evident, and more pronounced, in observations (e.g., Figure~~.~~ 3 in Goswami et al., 2023), which suggests an aerosol contribution to the IO warming pattern. Further analysis of the EU ensemble (Supplementary Figure S8~~not shown~~), shows that SST anomalies are largely anticorrelated with evaporation: reduced evaporation dominates the western and equatorial IO, while increases are seen in the south. Concurrently, anomalous near-surface divergent easterlies across the north-equatorial IO oppose the

climatological (south) westerlies, reducing evaporation and upwelling, which contribute to warming the SSTs. These patterns are similar to those associated with the Indian summer monsoon multi-decadal variability during the 20th century (Goswami et al., 2023). Also, the 55-year SST pattern resembles 20th-century-long changes, although the latter exhibits weaker anomalies and a less pronounced cooling (e.g., Rao et al., 2012; Roxy et al., 2014). Uncertainties remain in identifying the causes of the persistent western IO warming due to strong feedbacks between oceanic anomalies, atmospheric circulation, and convection (e.g., Rao et al., 2012; Swapna et al., 2014). While our findings highlight the role of remotely-forced wind anomalies, other mechanisms may also contribute. While SST anomalies and rainfall are anticorrelated in the long term, this relationship reverses in the early 20th century (~~Fig.~~ Figure 3 in Roxy et al., 2015), aligning with our findings.

Our results have important implications. They suggest that non-local anthropogenic aerosols have contributed significantly to shaping monsoon variability even during the early historical period. This is particularly relevant for understanding regional-scale impacts of anthropogenic forcing, which remain uncertain due to the spatial heterogeneity of emissions and their diverse climate effects. Importantly, under the current continued decrease in European aerosol emissions, assuming an opposite ASM response to the one described above, remotely-driven precipitation anomalies may significantly modulate, if not partially offset, the response to Asian aerosol emission changes (already declining or expected to do so in the future; e.g., Lund et al., 2019; Xiang et al. 2023). For example, assuming linearity in the combined responses, the abatement of EU sulphate aerosols would lead to a weaker monsoon over most of South Asia, and India in particular, which is opposite to the expected wetting associated with decreased sulphate aerosols over both South and East Asia (e.g., Bartlett et al., 2018). Conversely, EU aerosol reductions would contribute to further amplify the reversed SFND pattern over China brought about by decreased East Asian aerosol alone (e.g., Dong et al., 2016), resulting, for example, in enhanced drying over southeastern China. While the future monsoon response to the projected decline in worldwide aerosol emissions will most likely result from non-linear interactions among the different aerosol source regions, the above picture illustrates the complex interplay among local and remote aerosols and the need for a consistent and coordinated modelling and analysis approach (e.g., Wilcox et al., 2023).

While our analysis emphasises the central role of European aerosols, other remote emissions (e.g., from North America) and external forcings (e.g., greenhouse gases) may have also played a role. Our conclusions are based

on ensemble experiments comprising eight members each, consistent with the minimum number typically recommended for detecting forced multi-decadal signals (e.g., Deser et al., 2012). However, internal variability cannot be ruled out, and studies have, for example, discussed the association of Atlantic slow-frequency variability with the ISM multi-decadal mode (e.g., Rajesh and Goswami, 2020). In this context, the use of large single-forcing ensembles (e.g., Smith et al., 2022; Simpson et al., 2023) offers a promising approach to disentangling the individual contributions of greenhouse gases, anthropogenic aerosols and other external drivers. Furthermore, our findings are based on a single climate model and therefore depend on its representation of aerosol-cloud-radiation and circulation interactions. Given the well-known uncertainties in aerosol forcing and its climatic effects, the response may differ across models and from real-world observations. For example, CESM1 is known to exhibit a relatively strong aerosol effective radiative forcing (Zelinka et al., 2014; 2023), which may result in a stronger climate response to aerosol perturbations than seen in other models.

Acknowledgements. MAB acknowledges support from the Natural Environment Research Council (NE/N006038/1) and the Research Council of Norway (grant no. 324182; CATHY).

Data availability. GPCC data are retrieved from https://psl.noaa.gov/data/gridded/data.gpcc.html, CRU data from https://crudata.uea.ac.uk/cru/data/hrg/, and UDEL data from https://psl.noaa.gov/data/gridded/data.UDel_AirT_Precip.html. The ERA5 data are obtained at https://cds.climate.copernicus.eu/datasets/reanalysis-era5-pressure-levels-monthly-means. HadISST data are available from https://www.metoffice.gov.uk/hadobs/hadisst/, while the HadSLP2 dataset is accessed from https://www.metoffice.gov.uk/hadobs/hadslp2/. The CESM model data used in this study are available from MAB upon request.

Author contribution. WS and MAB designed the study. WS performed the analysis and completed the first draft of the manuscript. WS and MAB discussed the results, WA, MAB, and IC edited the manuscript. GW and YL provided suggestions on the analysis and interpretation of the results.

Competing interests. The authors have no competing interests to declare.

References

Allan, R., and Ansell, T.: A New Globally Complete Monthly Historical Gridded Mean Sea Level Pressure Dataset (HadSLP2): 1850–2004, J. Climate, 19, https://doi.org/10.1175/JCLI3937.1, 2006.

Andrews, T., and Forster, P.M.: Energy budget constraints on historical radiative forcing, Nat. Clim. Chang. 10, https://doi.org/10.1038/s41558-020-0696-1, 2020.

Bartlett, R. E., Bollasina, M. A., Booth, B. B. B. et al.: Do differences in future sulfate emission pathways matter for near-term climate? A case study for the Asian monsoon, Clim. Dynam., 50, https://doi.org/10.1007/s00382-017-3726-6, 2018.

Bellouin, N., et al.: Bounding aerosol radiative forcing of climate change, Rev. Geophys., 58, https://doi.org/10.1029/2019RG000660, 2020.

Bollasina, M.A, Ming, Y, Ramaswamy, V.: Anthropogenic aerosols and the weakening of the South Asian summer monsoon, Science, 334, https://doi.org/10.1126/science.1204994, 2011.

Bollasina, M. A., Ming, Y., Ramaswamy, V., Schwarzkopf, M. D., and Naik, V.: Contribution of local and remote anthropogenic aerosols to the twentieth century weakening of the South Asian monsoon, Geophys. Res. Lett., 41, https://doi.org/10.1002/2013GL058183, 2014.

Boucher, O., Randall, D., Artaxo, P., Bretherton, C., Feingold, G., Forster, P., Kerminen, V.-M., Kondo, Y., Liao, H., Lohmann, U., Rasch, P., Satheesh, S., Sherwood, S., Stevens, B., and Zhang, X.: Clouds and aerosols, in Climate change 2013: The physical science basis. Contribution of Working Group I to the Fifth Assessment Report of the Intergovernmental Panel on Climate Change, edited by Stocker T., Qin D., Plattner G.-K., Tignor M., Allen S., Boschung J., Nauels A., Xia Y., Bex V., and Midgley P., chap. 7, pp. 571–658, Cambridge University Press, Cambridge, United Kingdom and New York, NY, USA, https://10.1017/CBO9781107415324.016, 2013.

Cowan, T. and Cai, W.: The impact of Asian and non-Asian anthropogenic aerosols on 20th century Asian summer monsoon, Geophys. Res. Lett., 38, https://doi.org/10.1029/2011GL047268, 2011.

Deser, C., Phillips, A., Bourdette, V., et al.: Uncertainty in climate change projections: the role of internal variability, Clim. Dynam., 38, https://doi.org/10.1007/s00382-010-0977-x, 2012.

Dong, B., Sutton, R. T., Highwood, E. J., and Wilcox, L. J.: Preferred response of the East Asian summer monsoon to local and non-local anthropogenic sulphur dioxide emissions, Clim. Dynam., 46, https://doi.org/10.1007/s00382-015-2671-5, 2016.

Dong, B., Wilcox, L.J., Highwood, E.J., and Sutton, R. T.: Impacts of recent decadal changes in Asian aerosols on the East Asian summer monsoon: roles of aerosol–radiation and aerosol–cloud interactions, Clim. Dynam., 53, https://doi.org/10.1007/s00382-019-04698-0, 2019.

Enomoto, T., Hoskins, B.J., and Matsuda, Y.: The formation mechanism of the Bonin high in August, Q. J. Roy. Meteor. Soc., 129, https://doi.org/10.1256/qj.01.211, 2003.

Gadgil, S., and Rupa Kumar, K.: The Asian monsoon — agriculture and economy. In: The Asian Monsoon. Springer Praxis Books. Springer, Berlin, Heidelberg. https://doi.org/10.1007/3-540-37722-0_18, 2006.

Ghan, S. J., Liu, X., Easter, R. C., Zaveri, R., Rasch, P. J., et al.: Toward a minimal representation of aerosols in climate models: Comparative decomposition of aerosol direct, semidirect, and indirect radiative forcing, J. Climate, 25, https://doi.org/10.1175/JCLI-D-11-00650.1, 2012.

Goswami, D. J., Ashok, K., and Goswami, B. N.: Local ocean–atmosphere interaction in Indian summer monsoon multi-decadal variability, Clim. Dynam., 60, https://doi.org/10.1007/s00382-022-06377-z, 2023.

Guo, L., Highwood, E. J., Shaffrey, L. C., and Turner, A. G.: The effect of regional changes in anthropogenic aerosols on rainfall of the East Asian summer monsoon, Atmos. Chem. Phys., 13, https://doi.org/10.5194/acp-13-1521-2013, 2013.

Guo, L., Turner, A. G., and Highwood, E. J.: Impacts of 20th century aerosol emissions on the South Asian monsoon in the CMIP5 models, Atmos. Chem. Phys., 15, https://doi.org/10.5194/acp-15-6367-2015, 2015.

Harris, I., Jones, P.D., Osborn, T.J. and Lister, D.H.: Updated high-resolution grids of monthly climatic observations – the CRU TS3.10 Dataset, Int. J. Climatol., 34, https://doi.org/10.1002/joc.3711, 2014.

He, L., Zhou, T., and Chen, X.: South Asian summer rainfall from CMIP3 to CMIP6 models: biases and improvements, Clim. Dynam., 61, https://doi.org/10.1007/s00382-022-06542-4, 2023.

Hegerl G.C., Bronnimann S., et al.: Causes of climate change over the historical record, Environ. Res. Lett., 14, https://doi:10.1088/1748-9326/ab4557, 2019.

Hersbach, H., Bell, B., Berrisford, P., et al.: The ERA5 global reanalysis. Q. J. Roy. Meteor. Soc., 146, https://doi.org/10.1002/qj.3803, 2020.

Hoesly, R.M., et al.: Historical (1750–2014) anthropogenic emissions of reactive gases and aerosols from the Community Emissions Data System (CEDS), Geosci. Model Dev., 11, https://doi.org/10.5194/gmd-11-369-2018, 2018.

Huang, X., and Coauthors: The recent decline and recovery of Indian summer monsoon rainfall: relative roles of

external forcing and internal variability, J. Climate, 33, https://doi.org/10.1175/JCLI-D-19-0833.1, 2020.

Hurrell, J. W., Holland, M. M., Gent, P. R., Ghan, S., Kay, J. E., et al.: The Community Earth System Model, Bull. Amer. Met. Soc., 94, https://doi.org/10.1175/BAMS-D-12-00121.1, 2013.

Koffi, B., Dentener, F., Janssens-Maenhout, G., Guizzardi, D., Crippa, M., et al.: Hemispheric transport air pollution (HTAP): Specification of the HTAP2 experiments ensuring harmonized modelling (Tech. rep.) Luxembourg: Joint Research Centre JRC. https://doi.org/10.2788/725244, 2016.

Lau, W.K.M.: The aerosol-monsoon climate system of Asia: A new paradigm, J. Meteor. Res., 30, https://doi.org/10.1007/s13351-015-5999-1, 2016.

Li, X., Li, Q., Ding, Y., Yang, S., et al.: Possible influence of the interdecadal variation of the extratropical southern Indian Ocean SST on East Asian summer monsoon precipitation, Atmos. Res., 288, https://doi.org/10.1016/j.atmosres.2023.106721, 2023.

Li, X., Ting, M., Li, C., and Henderson, N.: Mechanisms of Asian summer monsoon changes in response to anthropogenic forcing in CMIP5 models, J. Climate, 28, https://doi.org/10.1175/JCLI-D-14-00559.1, 2015.

Li, Z., et al.: Aerosol and monsoon climate interactions over Asia, Rev. Geophys., 54, https://doi.org/10.1002/2015RG000500, 2016.

Li, J., Carlson, B.E., Yung, Y.L., et al.: Scattering and absorbing aerosols in the climate system, Nat. Rev. Earth Environ., 3, https://doi.org/10.1038/s43017-022-00296-7, 2022.

Liu, L., Shawki, D., Voulgarakis, A., Kasoar, M., Samset, B. H., et al.: A PDRMIP Multimodel study on the impacts of regional aerosol forcings on global and regional precipitation, J. Climate, 31, https://doi.org/10.1175/JCLI-D-17-0439.1, 2018.

Liu, Y., Cai, W., Sun, C., Song, H., Cobb, K. M., et al.: Anthropogenic aerosols cause recent pronounced weakening of Asian summer monsoon relative to last four centuries, Geophys. Res. Lett., 46, 5469–5479, https://doi.org/10.1029/2019GL082497, 2019.

Liu, Z., Bollasina, M. A., and Wilcox, L. J.: Impact of Asian aerosols on the summer monsoon strongly modulated by regional precipitation biases, Atmos. Chem. Phys., 24, 7227–7252, https://doi.org/10.5194/acp-24-7227-2024 , 2024.

Lu, R.-Y., Oh, J.H., and Kim, B.J.: A teleconnection pattern in upper-level meridional wind over the North African and Eurasian continent in summer, Tellus A, 54, https://doi.org/10.3402/tellusa.v54i1.12122, 2002.

Lund, M. T., Myhre, G., and Samset, B. H.: Anthropogenic aerosol forcing under the Shared Socioeconomic

Pathways, Atmos. Chem. Phys., 19, https://doi.org/10.5194/acp-19-13827-2019, 2019.

Meehl, G. A., and Arblaster, J. M.: GCM sensitivity experiments for the Indian monsoon and tropospheric biennial oscillation transition conditions, J. Climate, 15, https://doi.org/10.1175/1520-0442(2002)015<0923:imgset>2.0.co;2, 2002.

Meehl, G.A., Shields, C., Arblaster, J.M., Annamalai, H., and Neale, R.: Intraseasonal, seasonal, and interannual characteristics of regional monsoon simulations in CESM2, J. Adv. Model. Earth Sys., 12, https://doi.org/10.1029/2019MS001962, 2020.

Meehl, G. A., Shields, C. A., Arblaster, J. M., Fasullo, J., Rosenbloom, N., Hu, A., et al.: Processes that contribute to future South Asian monsoon differences in E3SMv2 and CESM2, Geophys. Res. Lett., 51, https://doi.org/10.1029/2024GL109056, 2024.

Neale, R. B., Gettelman, A., Park, S., Chen, C.-C., Lauritzen, P. H., et al.: Description of the NCAR Community Atmosphere Model (CAM 5.0), NCAR technical note, NCAR/TN-48, 274. https://doi.org/10.5065/D6N877R0, 2012.

Persad, G., Samset, B.H., Wilcox, L.J., Allen, R.J., Bollasina, M.A., et al.: Rapidly evolving aerosol emissions are a dangerous omission from near-term climate risk assessments, Environ. Res. Climate, 2, https://doi.org/10.1088/2752-5295/acd6af, 2023.

Preethi, B., Mujumdar, M., Kripalani, R.H. et al.: Recent trends and tele-connections among South and East Asian summer monsoons in a warming environment, Clim. Dynam., 48, https://doi.org/10.1007/s00382-016-3218-0, 2017.

Rajesh, P. V., and Goswami, B. N.: Four-dimensional structure and sub-seasonal regulation of the Indian summer monsoon multi-decadal mode, Clim. Dynam., 55, https://doi.org/10.1007/s00382-020-05407-y, 2020.

Rao, S.A., Dhakate, A.R., Saha, S.K. et al.: Why is Indian Ocean warming consistently?, Climatic Change, 110, https://doi.org/10.1007/s10584-011-0121-x, 2012.

Rayner, N. A., Parker, D. E., Horton, E. B., Folland, C. K., Alexander, L. V., Rowell, D. P., Kent, E. C., and Kaplan, A.: Global analyses of sea surface temperature, sea ice, and night marine air temperature since the late nineteenth century, J. Geophys. Res., 108, https://doi.org/10.1029/2002JD002670, 2003.

Rodwell, M. J., and Hoskins, B. J.: Subtropical anticyclones and summer monsoons, J. Climate, 14, https://doi.org/10.1175/1520-0442(2001)014<3192:SAASM>2.0.CO;2, 2001.

Roxy, M. K., Ritika, K., Terray, P., and Masson, S.: The curious case of Indian Ocean warming. J. Climate, 27,

https://doi.org/10.1175/JCLI-D-14-00471.1, 2014.

Roxy, M., Ritika, K., Terray, P. et al.: Drying of Indian subcontinent by rapid Indian Ocean warming and a weakening land-sea thermal gradient, Nat. Commun., 6, https://doi.org/10.1038/ncomms8423, 2015.

Saha, A., and Ghosh, S.: Can the weakening of the Indian Monsoon be attributed to anthropogenic aerosols? Environ. Res. Commun., 1, https://doi:10.1088/2515-7620/ab2c65, 2019.

Salzmann, M., Weser, H., Cherian, R.: Robust response of Asian summer monsoon to anthropogenic aerosols in CMIP5 models, J. Geophys. Res. Atmos., 119, https://doi:10.1002/2014JD021783, 2014.

Salzmann, M., and Cherian, R.: On the enhancement of the Indian summer monsoon drying by Pacific multidecadal variability during the latter half of the twentieth century, J. Geophys. Res. Atmos., 120, https://doi:10.1002/2015JD023313, 2015.

Samset, B. H., et al.: Climate impacts from a removal of anthropogenic aerosol emissions. Geophys. Res. Lett., 45, https://doi.org/10.1002/2017GL076079, 2018.

Samset, B.H., Lund, M.T., Bollasina, M., et al.: Emerging Asian aerosol patterns. Nat. Geosci., 12, https://doi.org/10.1038/s41561-019-0424-5, 2019.

Schneider, U., Becker, A., Finger, P. et al.: GPCC's new land surface precipitation climatology based on quality-controlled in situ data and its role in quantifying the global water cycle, Theor. Appl. Climatol., 115, https://doi.org/10.1007/s00704-013-0860-x, 2014,

Shao, Z., Wang, H., Geng, Y.F., et al.: East Asian summer monsoon response to anthropogenic aerosols redistribution: contrasting 1950–1980 and 1980–2010 to understand the role of non-Asian forcing, Clim. Dynam., 62, https://doi.org/10.1007/s00382-023-07016-x, 2024.

Shawki, D., Voulgarakis, A., Chakraborty, A., Kasoar, M., and Srinivasan, J.: The South Asian monsoon response to remote aerosols: Global and regional mechanisms, J. Geophys. Res., 123, https://doi.org/10.1029/2018JD028623, 2018.

Simpson, I. R., and Coauthors: The CESM2 single-forcing large ensemble and comparison to CESM1: implications for experimental design. J. Climate, 36, https://doi.org/10.1175/JCLI-D-22-0666.1, 2023.

Smith, S. J., van Aardenne, J., Klimont, Z., Andres, R. J., Volke, A., and Delgado Arias, S.: Anthropogenic sulfur dioxide emissions: 1850–2005, Atmos. Chem. Phys., 11, https://doi.org/10.5194/acp-11-1101-2011, 2011.

Smith, D., Gillett, N. P., Simpson, I. R., Athanasiadis, P. J., Baehr, J., Bethke, I., et al.: Attribution of multi-annual to decadal changes in the climate system: The large ensemble single forcing model intercomparison project

(LESFMIP), Front. Clim., 4, https://doi.org/10.3389/fclim.2022.955414, 2022.

Song, F., Zhou, T., and Qian, Y.: Responses of East Asian summer monsoon to natural and anthropogenic forcings in the 17 latest CMIP5 models, Geophys. Res. Lett., 41, https://doi.org/10.1002/2013GL058705, 2014.

Stier, P., van den Heever, S.C., Christensen, M.W., et al.: Multifaceted aerosol effects on precipitation, Nat. Geosci., 17, https://doi.org/10.1038/s41561-024-01482-6, 2024.

Swapna, P., Krishnan, R., and Wallace, J.M: Indian Ocean and monsoon coupled interactions in a warming environment, Clim. Dynam., 42, https://doi.org/10.1007/s00382-013-1787-8, 2014.

Szopa, S., et al.: Short-Lived Climate Forcers. In Climate Change 2021: The Physical Science Basis. Contribution of Working Group I to the Sixth Assessment Report of the Intergovernmental Panel on Climate Change [Masson-Delmotte, V., P. Zhai, A. Pirani, S.L. Connors, C. Péan, S. Berger, N. Caud, Y. Chen, L. Goldfarb, M.I. Gomis, M. Huang, K. Leitzell, E. Lonnoy, J.B.R. Matthews, T.K. Maycock, T. Waterfield, O. Yelekçi, R. Yu, and B. Zhou (eds.)]. Cambridge University Press, Cambridge, United Kingdom and New York, NY, USA, pp. 817–922, https://doi.org/10.1017/9781009157896.008, 2021.

Takaya, K., and Nakamura, H.: A formulation of a phase-independent wave-activity flux for stationary and migratory quasigeostrophic eddies on a zonally varying basic flow, J. Atmos. Sci., 58, https://doi.org/10.1175/1520-0469(2001)058<0608:AFOAPI>2.0.CO;2, 2001.

Turner, A., and Annamalai, H.: Climate change and the South Asian summer monsoon, Nature Clim. Change 2, https://doi.org/10.1038/nclimate1495, 2012

Undorf, S., Bollasina, M., Booth, B., and Hegerl, G.: Contrasting the effects of the 1850-1975 increase in sulphate aerosols from North America and Europe on the Atlantic in the CESM, Geophys. Res. Lett., 45, https://doi.org/10.1029/2018GL079970, 2018.

Undorf, S., Polson, D., Bollasina, M. A., Ming, Y., Schurer, A., and Hegerl, G. C.: Detectable impact of local and remote anthropogenic aerosols on the 20th century changes of West African and South Asian monsoon precipitation, J. Geophys. Res., 123, https://doi.org/10.1029/2017JD027711, 2018.

Wang, Q., Wang, Z., and Zhang, H.: Impact of anthropogenic aerosols from global, East Asian, and non-East Asian sources on East Asian summer monsoon system, Atmos. Res., 183, https://doi.org/10.1016/j.atmosres.2016.08.023, 2017.

Wang, B., and Coauthors: Toward predicting changes in the land monsoon rainfall a decade in advance. J. Climate, 31, https://doi.org/10.1175/JCLI-D-17-0521.1, 2018.

584 Wang, Z., Mu, J., Yang, M., and Yu, X.: Reexamining the mechanisms of East Asian summer monsoon changes
585 in response to non–East Asian anthropogenic aerosol forcing. J. Climate, 33, https://doi.org/10.1175/JCLI-D-
586 19-0550.1, 2020.
587 Wang, Z., Lin, L., Xu, Y., et al.: Incorrect Asian aerosols affecting the attribution and projection of regional climate
588 change in CMIP6 models, npj Clim. Atmos. Sci., 4, https://doi.org/10.1038/s41612-020-00159-2, 2021.
589 Wang, Z., Feng, J., Diao, C., Li, Y., Lin, L., and Xu, Y.: Reduction in European anthropogenic aerosols and the
590 weather conditions conducive to $PM_{2.5}$ pollution in North China: a potential global teleconnection pathway,
591 Environ. Res. Lett., 16, https://doi.org/10.1088/1748-9326/ac269d, 2021.
592 Watanabe, M.: Asian jet waveguide and a downstream extension of the North Atlantic Oscillation, J. Climate, 17,
593 https://doi.org/10.1175/JCLI-3228.1, 2004.
594 Westervelt, D. M., Conley, A. J., Fiore, A. M., Lamarque, J.-F., Shindell, D. T., Previdi, M., Mascioli, N. R.,
595 Faluvegi, G., Correa, G., and Horowitz, L. W.: Connecting regional aerosol emissions reductions to local and
596 remote precipitation responses, Atmos. Chem. Phys., 18, 12461–12475, https://doi.org/10.5194/acp-18-
597 12461-2018, 2018.
598 Wilcox, L. J., Allen, R. J., Samset, B. H., Bollasina, M. A., et al.: The Regional Aerosol Model Intercomparison
599 Project (RAMIP), Geosci. Model Dev., 16, https://doi.org/10.5194/gmd-16-4451-2023, 2023.
600 Wilcox L. J., Liu, Z., Samset, B. H., et al.: Accelerated increases in global and Asian summer monsoon
601 precipitation from future aerosol reductions, Atmos. Chem. Phys., 20, https://doi.org/10.5194/acp-20-11955-
602 2020, 2020.
603 Willmott, C. J., and Matsuura, K.: Smart interpolation of annually averaged air temperature in the United States,
604 J. Appl. Meteor. Climatol., 34, https://doi.org/10.1175/1520-0450(1995)034<2577:SIOAAA>2.0.CO;2,
605 1995.
606 Wu, G. X., Li, Z. Q., Fu, C. B., Zhang, X. Y., Zhang, R. Y., Zhang, R. H., et al.: Advances in studying interactions
607 between aerosols and monsoon in China. Science China Earth Sciences, 59, https://doi.org/10.1007/s11430-
608 015-5198-z, 2016.
609 Xiang, B., Xie, S. P., Kang, S. M. et al.: An emerging Asian aerosol dipole pattern reshapes the Asian summer
610 monsoon and exacerbates northern hemisphere warming, npj Clim. Atmos. Sci., 6,
611 https://doi.org/10.1038/s41612-023-00400-8, 2023.
612 Xie, P., and Arkin, P. A.: Global precipitation: A 17-Year monthly analysis based on gauge observations, satellite

613 estimates, and numerical model outputs, Bull. Amer. Meteor. Soc., 78, https://doi.org/10.1175/1520-
614 0477(1997)078<2539:GPAYMA>2.0.CO;2, 1997.
615 Zelinka, M. D., Andrews, T., Forster, P. M., and Taylor, K. E.: Quantifying components of aerosol-cloud-radiation
616 interactions in climate models, J. Geophys. Res. Atmos., 119, https://doi:10.1002/2014JD021710, 2014.
617 Zelinka, M. D., Smith, C. J., Qin, Y., and Taylor, K. E.: Comparison of methods to estimate aerosol effective
618 radiative forcings in climate models, Atmos. Chem. Phys., 23, https://doi.org/10.5194/acp-23-8879-2023,
619 2023.
620 Zhang, L., and Zhou, T.: An assessment of monsoon precipitation changes during 1901–2001. Clim. Dynam., 37,
621 https://doi.org/10.1007/s00382-011-0993-5, 2011.
622

Figures

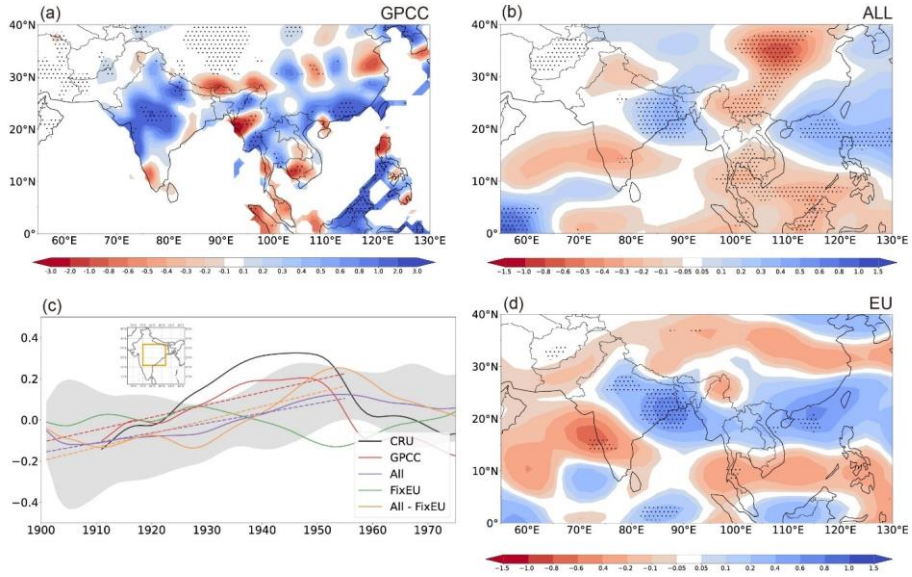

Figure 1. (a)-(b): Spatial patterns of the 1901-1955 linear trends of JJA precipitation (mm day^{-1} (55 years)$^{-1}$) for (a) GPCC, (b) the all-forcing ensemble (ALL), and (d) the difference between ALL and the all-forcing experiment with fixed preindustrial aerosol emissions over Europe (fixEU), representing the impact of EU aerosols. The black dots mark the grid points for which the trend exceeds the 90% significance level according to the two-tailed Student's t-test. (c): Time series of area-averaged JJA precipitation anomalies (mm day^{-1}; deviations from the 1901-2000 climatology) over central-northern India (land-only points within 75°–87°E, 16°–27°N; area shown in inset map) smoothed with 11-year running means to highlight low-frequency (multi-decadal) fluctuations. The black and red lines represent observations (CRU and GPCC, respectively), while the purple, green and orange lines represent the ensemble means of ALL, fixEU, and their difference (EU). The grey shading represents the standard deviation of the eight-member ALL ensemble around the mean. The 1901-1955 least-squares linear trends of the simulated time series are shown as dashed lines in the corresponding colours. Note that the interval for the simulated changes is half of that used for the observations.

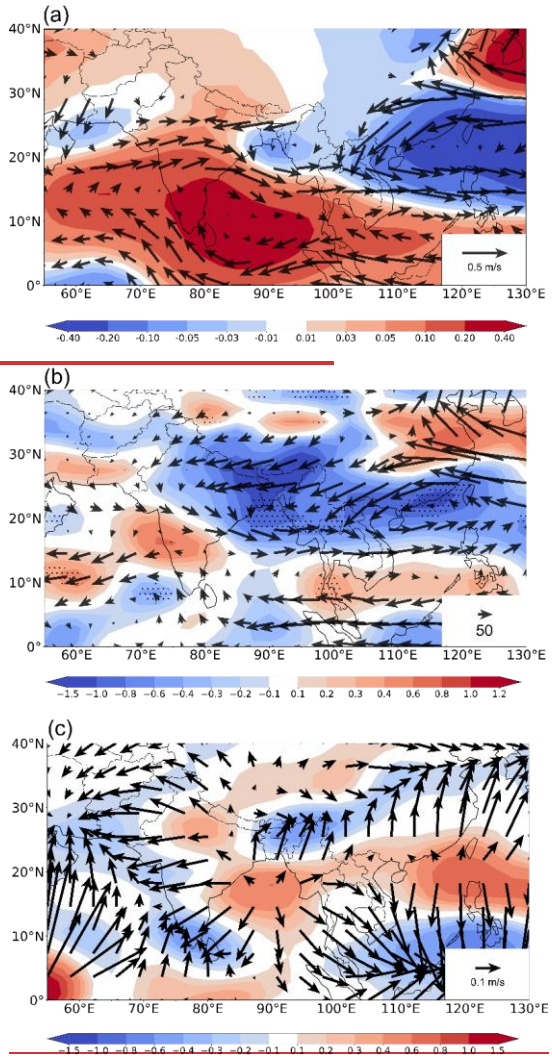
(a)
40°N
30°N
20°N
10°N
0°
60°E 70°E 80°E 90°E 100°E 110°E 120°E 130°E
0.5 m/s
-0.40 -0.20 -0.10 -0.05 -0.03 -0.01 0.01 0.03 0.05 0.10 0.20 0.40
(b)
40°N
30°N
20°N
10°N
0°
60°E 70°E 80°E 90°E 100°E 110°E 120°E 130°E
50
−1.5 −1.0 −0.8 −0.6 −0.4 −0.3 −0.2 −0.1 0.1 0.2 0.3 0.4 0.6 0.8 1.0 1.2
(c)
40°N
30°N
20°N
10°N
0°
60°E 70°E 80°E 90°E 100°E 110°E 120°E 130°E
0.1 m/s
−1.5 −1.0 −0.8 −0.6 −0.4 −0.3 −0.2 −0.1 0.1 0.2 0.3 0.4 0.6 0.8 1.0 1.5

641

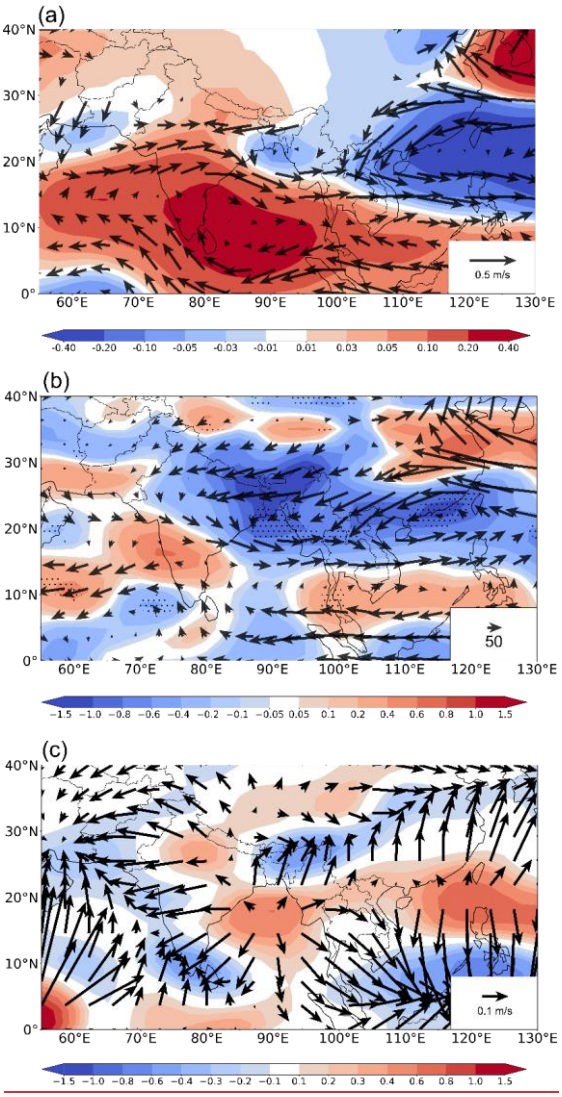

Figure 2. Spatial patterns of the 1901-1955 linear trends of the JJA average (a) 850-hPa winds (m s^{-1} (55 years)$^{-1}$) and 925-hPa streamfunction (colors, 10^6 m^2 s^{-1} (55 years)$^{-1}$), (b) 1000-300 hPa vertically integrated moisture transport (vectors, Kg m^{-1} s^{-1}) and its divergence (shades, mm d^{-1} (55 years)$^{-1}$), (c) 150-hPa divergent circulation (m s^{-1} (55 years)$^{-1}$) and its divergence (shades; 10^{-6} s^{-1} (55 years)$^{-1}$) associated with increased European sulphate aerosols (difference between the ALL and fixEU ensemble means). The black dots in (b) mark the grid points for which the trend exceeds the 90% significance level according to the two-tailed Student's t-test.

Formatted: Centered

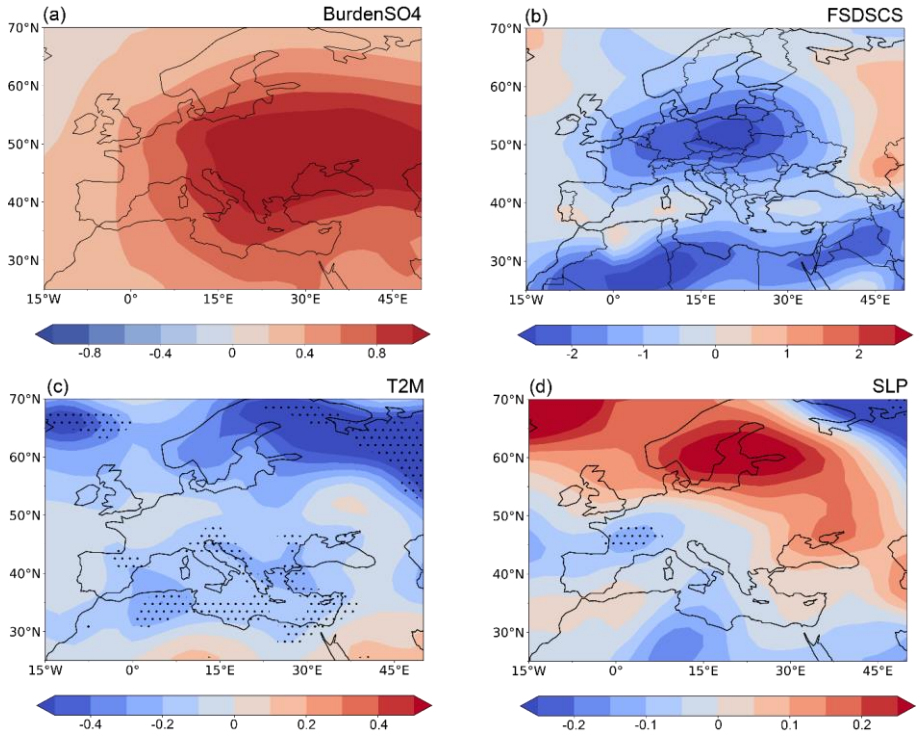

Figure 3. Spatial patterns of the 1901-1955 linear trends of the JJA average (a) column sulphate aerosol burden (10^{-5} kg m^{-2} (55 years)$^{-1}$), (b) surface clear-sky downward shortwave radiation (W m^{-2} (55 years)$^{-1}$), (c) 2-m air temperature (K (55 years)$^{-1}$), and (d) sea level pressure (hPa (55 years)$^{-1}$) associated with increased European sulphate aerosols (difference between the ALL and fixEU ensemble means). The black dots in (c) and (d) mark the grid points for which the trend exceeds the 90% significance level according to the two-tailed Student's t-test.

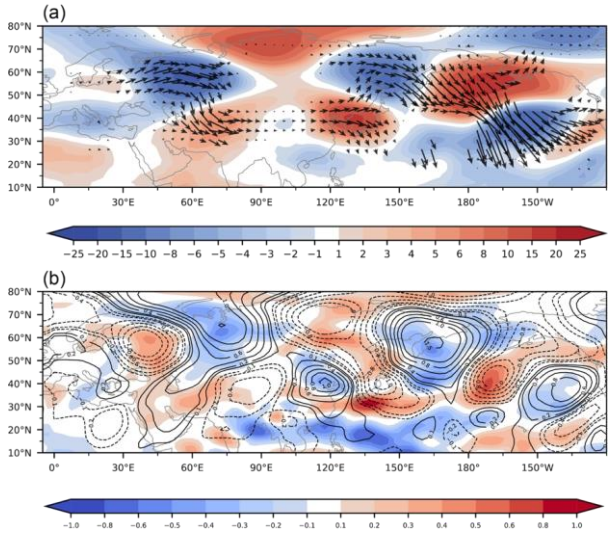

Figure 4. Spatial patterns of the 1901-1955 linear trends of the JJA average (a) 300-hPa wave activity flux (vectors; 10^{-4} m^2 s^{-2} (55 years)$^{-1}$) and streamfunction (shades; 10^5 m^2 s^{-1} (55 years)$^{-1}$), and (b) 300-hPa meridional wind (contours; m s^{-1} (55 years)$^{-1}$) and 500-hPa vertical velocity (shades; 10^{-2} Pa s^{-1} (55 years)$^{-1}$) associated with increased European sulphate aerosols (difference between the ALL and fixEU ensemble means).